

FAKE MASSIVE BLACK HOLES IN THE MILLI-HERTZ GRAVITATIONAL-WAVE BAND

XIAN CHEN

Astronomy Department, School of Physics, Peking University, 100871 Beijing, China and
Kavli Institute for Astronomy and Astrophysics at Peking University, 100871 Beijing, China

ZE-YUAN XUAN

Physics Department, School of Physics, Peking University, 100871 Beijing, China

PENG PENG

Astronomy Department, School of Physics, Peking University, 100871 Beijing, China

(Dated: March 20, 2020)
Draft version March 20, 2020

ABSTRACT

In gravitational wave (GW) astronomy accurate measurement of the source parameters, such as mass, relies on accurate waveform templates. Currently, the templates are developed assuming that the source, such as a binary black hole (BBH), is residing in a vacuum. However, astrophysical models predict that BBHs could form in gaseous environments, such as common envelopes, stellar cores, and accretion disks of active galactic nuclei. Here we revisit the impact of gas on the GW waveforms of stellar-mass BBHs with a focus on the early inspiral phase when the GW frequency is around milli-Hertz. We show that for these BBHs, gas friction could dominate the dynamical evolution and hence duplicate chirp signals. The relevant hydrodynamical timescale, τ_{gas} , could be much shorter than the GW radiation timescale, τ_{gw} , in the above astrophysical scenarios. As a result, the observable chirp mass is higher than the real one by a factor of $(1 + \tau_{\text{gw}}/\tau_{\text{gas}})^{3/5}$ if the gas effect is ignored in the data analysis. Such an error also results in an overestimation of the source distance by a factor of $(1 + \tau_{\text{gw}}/\tau_{\text{gas}})$. By performing matched-filtering analysis in the milli-Hertz band, we prove that the gas-dominated signals are practically indistinguishable from the chirp signals of those more massive BBHs residing in a vacuum environment. Such fake massive objects in the milli-Hertz band, if not appropriately accounted for in the future, may alter our understanding of the formation, evolution, and detection of BBHs.

Subject headings: Gravitational wave sources — Accretion — Active galactic nuclei — Hydrodynamics

1. INTRODUCTION

The majority of the black holes (BHs) detected by the ground-based gravitational wave (GW) observatories (i.e., LIGO and Virgo) turn out to be several times more massive than those previously detected in X-ray binaries (The LIGO Scientific Collaboration & the Virgo Collaboration 2019). Such a discrepancy has important implications for the formation and evolution of stellar-mass binary BHs (BBHs, Abbott et al. 2016). However, mass is not a direct observable in GW astronomy. It is inferred either from the chirp signal, i.e., an increase of the GW frequency with time, or from the merger and ringdown signals. If the signal gets distorted, either at the moment of generation or during the propagation, an error would be induced in the measurement of the mass.

Redshift is such a disturbing factor. It stretches the signal during its propagation. As a result, mass (m) is degenerate with redshift (z) so that one can only measure from GW signals the redshifted mass $m(1+z)$ (Schutz 1986). In two astrophysical scenarios, the mass-redshift degeneracy could lead to an significant overestimation of the masses of BBHs. In the first scenario, a BBH is at a high cosmological redshift and, nevertheless, is detected because the GW signal is magnified due to gravitational lensing (Broadhurst et al. 2018; Smith et al. 2018). So far, there is no convincing evidence supporting this scenario (Hannuksela et al. 2019). This scenario also has difficulties explaining the positive correlation

between the apparent masses and distances of the detected BBHs (The LIGO Scientific Collaboration & the Virgo Collaboration 2019). In the second scenario, the BBH is captured by a supermassive black hole (SMBH) to a small distance, so that Doppler and gravitational redshifts become significant, which then lead to the mass-redshift degeneracy (Chen & Han 2018; Chen et al. 2019). The uncertainty of this latter scenario lies mainly in the poor understanding of the event rate. In both scenarios the signal in the LIGO/Virgo band (centered around $10 - 10^2$ Hz) is similar to that of a not-redshifted, but more massive BBH. Distinguishing them would be difficult partly because the signal is short, which normally lasts no more than one second, too short to reveal any signature of gravitational lensing (Hannuksela et al. 2019) or a nearby SMBH (Chen et al. 2019).

The difficulty would be alleviated if the BBH can be detected by a space-borne GW observatory, such as the Laser Interferometer Space Antenna (LISA, Amaro-Seoane et al. 2017). LISA is sensitive to milli-Hertz (mHz) GWs and hence can capture a BBH at the early inspiral phase, weeks to millennia before it enters the LIGO/Virgo band (Miller 2002; Sesana 2016; Moore et al. 2019). Using the chirp signal, LISA can also measure the (redshifted) mass of the BBH. In this way, LISA may detect hundreds of massive BBHs during its mission duration of 4–5 years (Sesana 2016; Kyutoku & Seto 2016; Lamberts et al. 2018; Kremer et al. 2018) and compare their masses with those from LIGO/Virgo observations.

Moreover, by tracking the BBHs with a decent signal-to-noise ratio (SNR, e.g., > 10) for several months to years, LISA may reveal multiple images of a GW source if it is strongly lensed (Seto 2004; Sereno et al. 2011). The long signal may also reveal a shift of the GW phase caused by the wave effect of gravitational lensing (Nakamura 1998; Takahashi & Nakamura 2003). Moreover, if a BBH is close to a SMBH, the long waveform should also contain imprints of the orbital motion of the binary around the SMBH (Inayoshi et al. 2017; Meiron et al. 2017; Robson et al. 2018; Chamberlain et al. 2019; Tamanini et al. 2020; Wong et al. 2019; Torres-Orjuela et al. 2020) or the perturbation of the binary orbit by the tidal force of the SMBH (Meiron et al. 2017; Hoang et al. 2019; Randall & Xianyu 2019; Fang et al. 2019). These signatures can help us identify the BBHs affected by the redshift effects.

Redshift is not the only factor in GW astronomy that could affect the measurement of mass. Gas, for example, can exert a frictional force on a binary and hence lead to a faster orbital decay (Ostriker 1999; Kim & Kim 2007; Kim et al. 2008). The resulting GW signal is expected to differ from the real chirp signal due to GW radiation only. The impact on the mass measurement deserves further investigation since a large fraction of BBHs may form in gaseous environments. For example, BBHs can be produced by binary-star evolution, and in this case the mergers may happen inside a common envelope (Ivanova et al. 2013; MacLeod et al. 2017; Ginat et al. 2020) or the fallback material from the previous supernovae (Tagawa et al. 2018). Moreover, some BBHs may form in the accretion disks of active galactic nuclei (AGNs, McKernan et al. 2012; Bartos et al. 2017; Stone et al. 2017). When these BBHs merge, it is likely that they are surrounded by dense gas. Furthermore, the dense cores of massive stars may also produce BBHs, and hence the mergers would also be accompanied by gas (Loeb 2016; Fedrow et al. 2017; D’Orazio & Loeb 2018). The density of the gas can reach $10^8 - 10^{14} \text{ cm}^{-3}$ in the case of AGN disks, $10^{16} - 10^{19} \text{ cm}^{-3}$ in common envelopes, and even higher in stellar cores (see Antoni et al. 2019, for a summary).

Several earlier works studied the impact of gas on the GW signal of merging binaries, including BBHs in the LIGO/Virgo band (Fedrow et al. 2017; Ginat et al. 2020; Cardoso & Maselli 2019) and extreme-mass-ratio inspirals (another type of binary composed of a stellar-mass BH orbiting a SMBH) in the LISA band (Yunes et al. 2011; Kocsis et al. 2011; Barausse et al. 2014). They focused on the final evolutionary stage when the semi-major axes (a) of the binaries are only $10 - 10^2$ times the Schwarzschild radius (r_S) of the bigger BHs. At this stage, GW radiation predominates and gas plays a minor role. Nevertheless, these works showed that gas could induce a small phase shift to the GW signal. The phase shift does not significantly affect the mass measurement but can be used to identify the mergers happening in gas.

The BBHs in the LISA band are very different from those considered in the earlier works. They have much greater semi-major axes ($a \sim 10^3 - 10^4 r_S$, e.g., Chen & Amaro-Seoane 2017) since GW frequency is proportional to $a^{-3/2}$. Such wide binaries have much weaker GW radiation because the GW power scales with a^{-5} (Peters 1964). Consequently, gas could play a dominant role in the evolution of these binaries and, in this way, produce a fake chirp signal. If this factor is not accounted for in the LISA data analysis, one may overestimate the masses, as we have shown in one example of our

preliminary study (Chen & Shen 2019, Paper I).

Here we present our full analysis of the problem and discuss the detectability of such “fake” massive BBHs in the LISA band. The paper is organized as follows. In §2 we explain how mass is measured from a chirp signal and why it is affected by gas friction. Then in §3 we show that in realistic astrophysical scenarios gas friction indeed can overcome GW radiation and dominate the orbital evolution of an inspiraling BBH. We compute the gas-dominated chirp signals in §4 and show that they resemble the chirp signals from more massive BBHs in vacuum environments. In §5, we employ the “matched-filtering” technique to quantify the similarity between the chirp signals in the cases with and without gas. Finally, in §6 we discuss the detectability of the fake massive BBHs in the LISA band.

2. CHIRP SIGNAL AND THE EFFECT OF GAS

We focus on the early inspiral phase because the majority of the LISA BBHs are in this evolutionary phase. Without gas, the semi-major axis a of a BBH decays approximately as

$$\dot{a} = \dot{a}_{\text{gw}} := \frac{64 G^3 m_1 m_2 m_{12}}{5 c^5 a^3} \quad (1)$$

(Peters 1964, assuming near-Keplerian circular orbits), where the dot symbol denotes the time derivative, G is the gravitational constant, c is the speed of light, m_1 and m_2 are the masses of the two BH members, and $m_{12} = m_1 + m_2$ is the total mass of the binary. During the orbital decay, the GW frequency, which can be calculated with $f = \pi^{-1}(Gm_{12}/a^3)^{1/2}$, increases at a rate of $\dot{f} \propto f^{11/3}$. Such a characteristic signature is called the “chirp signal”. From it, one can derive a characteristic mass scale

$$\mathcal{M} = \frac{c^3}{G} \left(\frac{5f^{-11/3} \dot{f}}{96\pi^{8/3}} \right)^{3/5} = \frac{(m_1 m_2)^{3/5}}{(m_1 + m_2)^{1/5}}, \quad (2)$$

which is known as the “chirp mass”. It uniquely determines the time evolution of f .

From the chirp signal one can also derive the distance d of the BBH (Schutz 1986). This is because from f and \dot{f} one can infer the energy-loss rate of the orbit, $\dot{E} \propto f^{-4} \dot{f}^2$, which also equals the GW power. In addition, the frequency f and the GW amplitude h , together, determine a flux $S \propto h^2 f^2$ which is the GW flux. From the power and the flux, one can derive the distance of the source

$$d = \frac{4G}{c^2} \frac{\mathcal{M}}{h} \left(\frac{G}{c^3} \pi f \mathcal{M} \right)^{2/3}. \quad (3)$$

If the BBH is at a cosmological distance, the mass and distance encoded in the chirp signal will have slightly different meanings. First, both f and \dot{f} will be distorted by the redshift so that the observed frequency becomes $f_o = f(1+z)^{-1}$ and the chirping rate appears to be $\dot{f}_o = \dot{f}(1+z)^{-2}$. As a result, the chirp mass that one will derive from the redshifted GW signal becomes

$$\mathcal{M}_o := \frac{c^3}{G} \left(\frac{5f_o^{-11/3} \dot{f}_o}{96\pi^{8/3}} \right)^{3/5} = \mathcal{M}(1+z). \quad (4)$$

This apparent chirp mass is bigger than the intrinsic one by a redshift factor $1+z$. Second, the GW amplitude will be determined by the transverse comoving distance d_C in the fol-

lowing way,

$$h_o = \frac{4G}{c^2} \frac{M}{d_C} \left(\frac{G}{c^3} \pi f M \right)^{2/3}. \quad (5)$$

If one uses the observed f_o , \dot{f}_o , and h_o to infer a distance d_o , one will get

$$d_o = \frac{4G}{c^2} \frac{M_o}{h_o} \left(\frac{G}{c^3} \pi f_o M_o \right)^{2/3} = d_C(1+z). \quad (6)$$

Such a distance is identical to the luminosity distance d_L in a Λ CDM cosmology.

Gas will accelerate the orbital shrinkage and, in this way, affect the chirp signal. Because of the gas friction (or viscosity, e.g., Haiman et al. 2009), a BBH would shrink at a faster rate of $\dot{a} = \dot{a}_{\text{gw}} + \dot{a}_{\text{gas}}$, where the additional term, $\dot{a}_{\text{gas}} < 0$, is due to gas. Correspondingly, \dot{f}_o increases more rapidly, as

$$\frac{\dot{f}_o}{f_o} = -\frac{3}{2} \left[\frac{\dot{a}_{\text{gw}} + \dot{a}_{\text{gas}}}{a(1+z)} \right]. \quad (7)$$

The apparent increase of \dot{f}_o will lead to an overestimation of the mass of the BBH, as well as the distance. To see this effect, it is useful to first define an acceleration factor

$$\Gamma := \dot{a}_{\text{gas}}/\dot{a}_{\text{gw}}. \quad (8)$$

From this definition, it follows that $\dot{f}_o = (1+\Gamma)(1+z)^{-2}\dot{f}$, i.e., the chirp signal evolves faster by a factor of $1+\Gamma$. Finally, by revisiting Equations (4) and (6), we find that the apparent mass and distance become

$$M_o = (1+\Gamma)^{3/5} M(1+z), \quad (9)$$

$$d_o = (1+\Gamma) d_C(1+z) = (1+\Gamma) d_L. \quad (10)$$

The factor Γ in general is a function of a , because both \dot{a}_{gw} and \dot{a}_{gas} depend on a . Such a dependence has two consequences. (i) If the semi-major axis changes substantially during the observational period, one would see a significant variation of M_o and d_o with time. This result is inconsistent with the dynamical evolution of a BBH in a vacuum, and hence can be used to prove the presence of an environmental factor, such as gas. (ii) Otherwise, if a evolves very slowly, i.e., the corresponding evolutionary timescale $a/|\dot{a}_{\text{gw}} + \dot{a}_{\text{gas}}|$ is much longer than the observational period T_{obs} , the acceleration factor Γ would be more or less a constant. In this case, the measurement of M_o and d_o would be relatively consistent during the observational period, and both values would be greater than the intrinsic ones.

For LIGO/Virgo, the relevant BBHs are normally in the first case because the signal is typically less than a second but each LIGO/Virgo observing run lasts several weeks to several months. This is why the previous studies found that the gas effect could be discerned in the LIGO/Virgo waveforms (see §1). For LISA, however, the majority of the in-band BBHs belong to the latter case because a BBH could dwell in the band for as long as millions of years but the canonical mission duration of LISA is only 4–5 years. During such a short observing time, Γ is almost constant so that discerning the gas effect is more difficult. An overestimation of the mass and distance becomes more likely.

3. HYDRODYNAMICS VERSUS GW RADIATION

To evaluate the efficiency of the hydrodynamical drag, we compare the GW radiation timescale, defined as $\tau_{\text{gw}} :=$

$|a/\dot{a}_{\text{gw}}|$, and the hydrodynamical timescale, defined as $\tau_{\text{gas}} := |a/\dot{a}_{\text{gas}}|$. Following these definitions, the acceleration factor Γ equals $\tau_{\text{gw}}/\tau_{\text{gas}}$. Because the most sensitive band of LISA is around 3 mHz, the corresponding BBHs have a typical semi-major axis of

$$a = \left(\frac{Gm_{12}}{\pi^2 f^2} \right)^{1/3} \simeq 0.0021 \left(\frac{m_{12}}{20 M_\odot} \right)^{1/3} \left(\frac{f}{3 \text{ mHz}} \right)^{-2/3} \text{ AU}. \quad (11)$$

According to Equation (1), without gas these binaries have a typical evolutionary timescale of

$$\tau_{\text{gw}} = \frac{5}{64} \frac{c^5 a^4}{G^3 m_1 m_2 m_{12}} \quad (12)$$

$$\simeq \frac{9.1 \times 10^3}{q(1+q)^{-1/3}} \left(\frac{m_1}{10 M_\odot} \right)^{-5/3} \left(\frac{f}{3 \text{ mHz}} \right)^{-8/3} \text{ years}, \quad (13)$$

where q denotes the mass ratio m_2/m_1 of the two BHs (we assume $m_1 \geq m_2$).

As for τ_{gas} , we first use the hydrodynamic drag derived in Ostriker (1999); Sánchez-Salcedo & Brandenburg (1999) to estimate its value. The drag force on the secondary BH (m_2) is calculated with $F \sim 4\pi\rho(Gm_2/v)^2$, where ρ is the mass density of the background gas and v is the Kepler velocity of the secondary. For circular orbits, we have $v \propto a^{-1/2}$, so that $a/\dot{a}_{\text{gas}} = -v/(2\dot{v})$. Moreover, since $|\dot{v}| = F/m_2$, we derive that

$$\tau_{\text{gas}} = \frac{m_2 v}{2F} \simeq \frac{1.1 \times 10^4}{q(1+q)^2} \left(\frac{n}{10^{16} \text{ cm}^{-3}} \right)^{-1} \left(\frac{f}{3 \text{ mHz}} \right) \text{ yrs}, \quad (14)$$

where n is the number density of hydrogen atoms in the gas background. It follows that

$$\Gamma \simeq 4.3 \left(\frac{1+q}{2} \right)^{7/3} \left(\frac{n}{10^{16} \text{ cm}^{-3}} \right) \left(\frac{m_1}{10 M_\odot} \right)^{-5/3} \left(\frac{f}{3 \text{ mHz}} \right)^{-11/3}. \quad (15)$$

In the above derivation of τ_{gas} , it is assumed that the gas background is homogeneous and the small body is moving in a straight line. However, for the BHs in binaries, which move along Keplerian orbits, it has been shown that the formula for the drag force will be modified, because the shape of the density wake is different (Sánchez-Salcedo & Brandenburg 2001; Escala et al. 2004; Kim & Kim 2007; Kim et al. 2008). More recently, Antoni et al. (2019) showed that when a is smaller than the Bondi accretion radius $R_{\text{acc}} = Gm_{12}/c_s^2$ (c_s being the sound speed of the gas medium), the gas density close to the binary will be much higher than the background density due to accretion. This is normally the case for those BBHs embedded in common envelopes and AGN accretion disks. If we use $\tilde{n} \sim n(R_{\text{acc}}/a)^{3/2}$ to correct the gas density around the binary (Bondi 1952; Antoni et al. 2019), we find that the timescale due to hydrodynamical drag becomes

$$T_{\text{gas}} \simeq 8.5 \times 10^4 q^{-1} (1+q)^{-3} \left(\frac{n}{10^{11} \text{ cm}^{-3}} \right)^{-1} \times \left(\frac{m_1}{10 M_\odot} \right)^{-1} \left(\frac{c_s}{10^2 \text{ km s}^{-1}} \right)^3 \text{ years}. \quad (16)$$

Note that the new timescale does not depend on a or f . A similar result can be found in (Bartos et al. 2017, see their Fig. 2). Moreover, in the last equation we have rescaled n

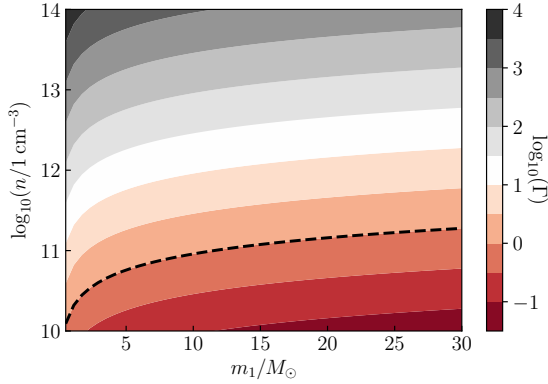


FIG. 1.— Dependence of the acceleration factor, calculated in Eq. (17), on the mass of the primary BH, m_1 , and the gas density n . The other model parameters are set to $f = 3$ mHz, $q = 1$, and $c_s = 10^2$ km s $^{-1}$. The black dashed curve marks the location where $\Gamma = 1$.

with 10^{11} cm $^{-3}$. Given this timescale, we derive that

$$\Gamma \approx 1.1 \left(\frac{1+q}{2} \right)^{10/3} \left(\frac{n}{10^{11} \text{ cm}^{-3}} \right) \times \left(\frac{m_1}{10 M_\odot} \right)^{-2/3} \left(\frac{c_s}{10^2 \text{ km s}^{-1}} \right)^{-3} \left(\frac{f}{3 \text{ mHz}} \right)^{-8/3}. \quad (17)$$

For illustrative purposes, we show in Figure 1 the dependence of the Γ computed in the last equation on m_1 and n . The black dashed curve marks the location where $\Gamma = 1$. Above it, gas dominates the dynamical evolution of a BBH, and hence the chirp signal is determined by gas dynamics, not GW radiation.

Equations (15) and (17) suggest that for LIGO/Virgo BBHs, which typically have $m_1 \sim 10 M_\odot$ and $f \sim 10^2$ Hz, the gas effect is negligible unless the gas density n is orders of magnitude higher than 10^{16} cm $^{-3}$. This is the reason that for LIGO/Virgo sources, significant gas effect is expected only in stellar cores, where n could be as high as $(10^{28} - 10^{31})$ cm $^{-3}$ (e.g. Fedrow et al. 2017). For LISA sources with $f \sim 3$ mHz, however, gas effect is already important when $n \sim 10^{16}$ cm $^{-3}$ according to Equation (15) or $n \sim 10^{12}$ cm $^{-3}$ according to Equation (17). These two characteristic densities can be found, respectively, in common envelopes and AGN accretion disks (e.g. Antonini et al. 2019). Therefore, the gaseous environments common for BBHs would affect the LISA signals more than the LIGO/Virgo ones.

4. FAKING A CHIRP SIGNAL

Having understood the effect and the relative importance of gas, we now compute the chirp signal of a BBH embedded in a gaseous environment. In the following, we assume $z = 0$ for simplicity ($f_o = f$). When there is no gas, we calculate the time derivative of the GW frequency (\dot{f}_{gw}) using a 3.5 post-Newtonian (PN) approximation presented in Sathyaprakash & Schutz (2009). When gas is present, we have $\dot{f}_o = \dot{f}_{\text{gw}} + \dot{f}_{\text{gas}}$, where \dot{f}_{gas} is calculated with $\dot{f}_{\text{gas}} = -3f/(2\tau_{\text{gas}})$ according to Equation (7). In this way, the gas effect is included in the model through a parameter τ_{gas} .

Figure 2 compares the long-term evolution of the chirp signal in the cases with and without the gas drag. The blue solid curve corresponds to a $10 M_\odot - 10 M_\odot$ BBH ($\mathcal{M} \approx 8.7 M_\odot$) embedded in a gaseous medium. The two BHs coalesce at the time $t = t_c$. The hydrodynamical timescale τ_{gas} is computed according to Equation (16) and the model parameters are chosen such that $\tau_{\text{gw}}/\tau_{\text{gas}} = 10$ when $f = 3$ mHz. This

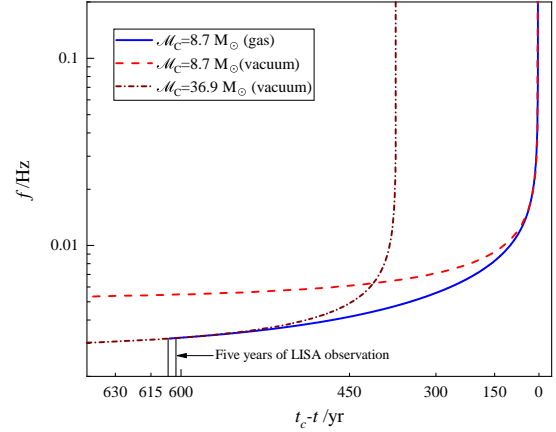


FIG. 2.— Evolution of the GW frequency as a function of the time before coalescence. The blue solid curve shows a $10 M_\odot - 10 M_\odot$ circular BBH embedded in a gaseous environment. The model parameters are chosen such that $\Gamma = 10$ when the GW frequency is $f = 3$ mHz (see Eq.(17)). The two vertical lines mark the typical LISA observational window of five years. The red dashed curve shows the chirp signal of the same BBH but placed in a vacuum. The coalescence times of the previous two BBHs are aligned for easier comparison. The dot-dashed curve shows another BBH merging in vacuum but with higher masses. It is offset in time so that the GW frequency in the LISA observational window is also 3 mHz.

chirp signal around $f = 3$ mHz, according to Equation (9), should resemble a more massive binary with a chirp mass of $(1 + \Gamma)^{3/5} \mathcal{M} \approx 37 M_\odot$ in a vacuum. The chirp signal of the latter more massive BBH is shown as the dot-dashed curve, and we can see that, indeed, at $f = 3$ mHz it matches the signal of the smaller binary embedded in gas. Eventually, the two signals diverge, since Γ is decreasing, but the divergence appears more than one hundred years later. If we focus on the LISA observational window of five years (marked by the two vertical lines), the two signals are almost identical. Finally, during the coalescence, the blue curve recovers the chirp signal of a $10 M_\odot - 10 M_\odot$ binary in a vacuum (red dashed curve), because GW radiation predominates during the merger.

To see more clearly the chirp signal in the observation window of LISA, we show in Figure 3 the evolution of f during a period of 1 – 2 years, around the moment when f is approximately 3 mHz. Now the chirp signals look like straight lines because the observational period is orders of magnitude shorter than the evolutionary timescales of the BBHs. Although the variation of f is small during the observation period, it is detectable by LISA because LISA’s resolution is approximately $10^{-8}(1 \text{ yr}/T_{\text{obs}})(10/\text{SNR})$ Hz (Seto 2002). Comparing the blue solid and the red dashed lines, we see that the presence of gas increases the slope of the chirp signal. The steeper line resembles the chirp signal of a more massive BBH in a vacuum with a chirp mass of $37 M_\odot$.

We have seen that with or without gas, the chirp signals in the LISA band are almost straight lines and are relatively featureless compared to those in the LIGO/Virgo band. This is the main reason that in this band a BBH in a gaseous environment could be misidentified as a more massive binary in a vacuum.

5. MISIDENTIFICATION

LISA uses a technique called “matched filtering” to search for BBHs in the data stream (Finn 1992; Cutler & Flanagan

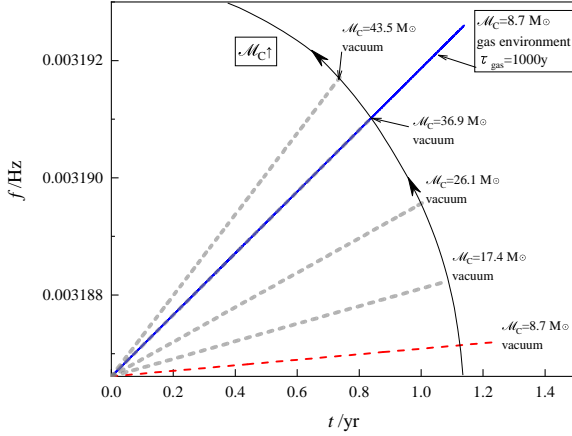


FIG. 3.— Chirp signals in the LISA observational window. The blue solid curve is computed with the gas effect and the red dashed one without. The model parameters are the same as in Fig. 2. The gray dashed curves show the dependence of the chirp signal on the chirp mass when there is no gas.

1994). In this section, we will show that this method cannot distinguish light BBHs embedded in certain gaseous environments from those massive ones in vacuum.

5.1. Matched filtering

Given two waveforms, h_1 and h_2 , their similarity is quantified by a “fitting factor” (FF), which is defined as

$$\text{FF} = \frac{\langle h_1 | h_2 \rangle}{\sqrt{\langle h_1 | h_1 \rangle \langle h_2 | h_2 \rangle}}. \quad (18)$$

The term $\langle h_1 | h_2 \rangle$ means an inner product of

$$\langle h_1 | h_2 \rangle = 2 \int_0^\infty \frac{\tilde{h}_1(f) \tilde{h}_2^*(f) + \tilde{h}_1^*(f) \tilde{h}_2}{S_n(f)} df, \quad (19)$$

where the tilde symbols stand for the Fourier transformation, the stars stand for the complex conjugation, and $S_n(f)$ is the spectral noise density of LISA (Klein et al. 2016). Identical waveforms have $\text{FF} = 1$.

In our problem, $h_1(t)$ is the chirp signal of a BBH embedded in a gaseous environment, and $h_2(t)$ is the waveform of an inspiraling BBH in a vacuum. By tuning the parameters of h_2 , we want to maximize the FF. We follow Cutler & Flanagan (1994) and compute the waveforms using

$$h(t) = \frac{Q(\theta, \varphi, \psi, \iota) \mu M}{d_L a(t)} \cos\left(\int 2\pi f dt\right), \quad (20)$$

where $Q(\theta, \varphi, \psi, \iota)$ is a function depending on the sky location and orientation of the BBH. In the integrand, the frequency f is a function of a . It is computed using the 3.5 PN approximation for h_2 (Sathyaprakash & Schutz 2009) and using the gas model described in §4 for h_1 .

Because the two evolutionary timescales τ_{gas} and τ_{gw} are both much longer than the observational period of LISA, f is almost a constant in our model. In this case the computation of the inner product $\langle h_1 | h_2 \rangle$ can be performed in the time domain and the calculation of the FF can be simplified. First, the noise curve $S_n(f)$ can be taken out of the integration because

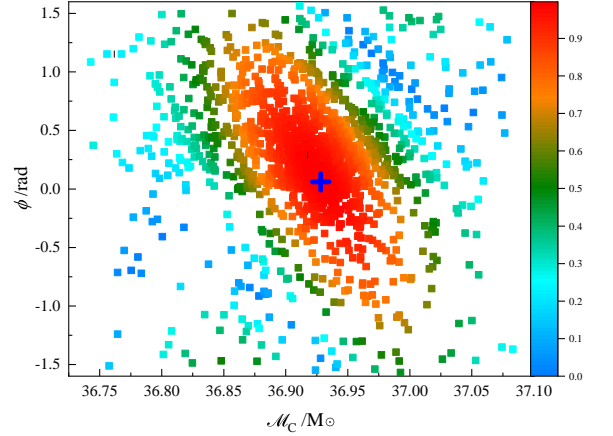


FIG. 4.— Dependence of the FF on the chirp mass \mathcal{M}_c and initial phase ϕ of the template h_2 . The dependence on q is relatively weak and is not shown here. The signal h_1 is generated using the parameters $\mathcal{M}_c = 8.7 M_\odot$, $q = 0.7$, and $\tau_{\text{gas}} = 10^3$ years. The plus symbol marks the location of the maximum FF, which is offset from the real chirp mass ($8.7 M_\odot$).

of the small variation of f , so that

$$\langle h_1 | h_2 \rangle \approx \frac{2}{S_n} \int_0^\infty [\tilde{h}_1^*(f) \tilde{h}_2(f) + \tilde{h}_1(f) \tilde{h}_2^*(f)] df. \quad (21)$$

Second, using Parseval’s theorem, we further derive

$$\langle h_1 | h_2 \rangle \approx \frac{4}{S} \int_0^\infty h_1(t) h_2(t) dt. \quad (22)$$

Finally, the FF can be written as

$$\text{FF} = \frac{\int_0^\infty h_1(t) h_2(t) dt}{\sqrt{\int_0^\infty h_1(t) h_1(t) dt \int_0^\infty h_2(t) h_2(t) dt}}. \quad (23)$$

Note that there is no more dependence on d_L , $Q(\theta, \varphi, \psi, \iota)$, or $S_n(f)$, because they all cancel out. Given h_1 , i.e., the signal, we want to find a template h_2 that maximizes the FF. The parameter space in which we conduct this search is (\mathcal{M}_c, q, ϕ) , where ϕ is the initial phase.

5.2. Examples

Figure 4 shows one example of our search. The signal is generated using a BBH with $\mathcal{M}_c = 8.7 M_\odot$, $q = 0.7$, and a hydrodynamical timescale of $\tau_{\text{gas}} = 10^3$ years. Initially, the GW frequency is $f = 3$ mHz, and the corresponding GW radiation timescale is about 10^4 years. In this particular example the observational period is set to $T_{\text{obs}} = 1.25$ years, but later we will show the FF for different T_{obs} . We match the signal using the templates developed for vacuum BBHs, i.e., the 3.5 PN approximation described above. We use a simulated annealing algorithm to search for the highest FF in the parameter space of (\mathcal{M}_c, q, ϕ) . The best FF is found at a chirp mass of $\mathcal{M}_c \approx 37 M_\odot$. It is offset from the real chirp masses by a factor of about 4.2, which is consistent with our Equation (9). This result confirms our prediction that ignoring the gas effect could result in a significant overestimation of the mass of a LISA BBH.

We note that the best FF and the corresponding best-match \mathcal{M}_c are both functions of T_{obs} . Figure 5 shows such a de-

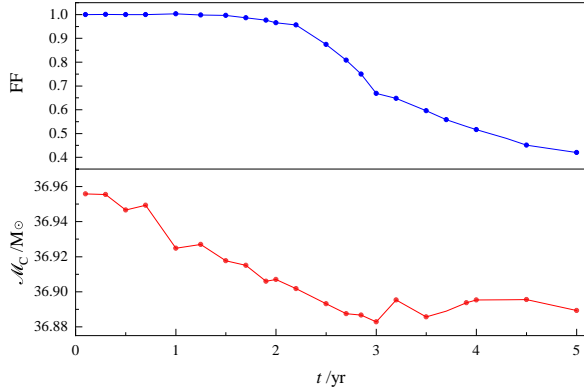


FIG. 5.— Variation of the maximum FF and the best-fit chirp mass with the observational period. The real chirp mass of the BBH is $8.7 M_{\odot}$.

pendence on time. The model parameters are the same as in Figure 4. During the first 1 – 2 years, the FF remains close to 1 and afterwards decreases with time. The FF deteriorates on a long timescale because the perturbation on the GW phase by the gas effect is accumulative. For the best-fit \mathcal{M}_c , it decreases with time but remains close to $37 M_{\odot}$.

Whether or not LISA is able to distinguish h_1 from h_2 depends on not only the FF but also the SNR, since noise also plays a role. The SNR is defined as

$$\text{SNR}^2 := \langle h|h \rangle. \quad (24)$$

According to Lindblom et al. (2008), two waveforms are distinguishable when $\langle \delta h | \delta h \rangle > 1$, where $\delta h := \tilde{h}_1(f) - \tilde{h}_2(f)$. This criterion can be simplified in our problem because we are often in a situation where $h_1 \simeq h_2$. In this case we have $\text{SNR}^2 \simeq \langle h_1 | h_1 \rangle \simeq \langle h_2 | h_2 \rangle$, and the criterion reduces to

$$\text{FF} < 1 - 1/(2 \text{SNR}^2). \quad (25)$$

If we take $\text{SNR} \simeq 10$ as the threshold for LISA to claim a detection, the corresponding criterion of distinguishing two different waveforms becomes $\text{FF} < 0.995$.

According to this criterion, the gas and vacuum waveforms used in Figure 5 are indistinguishable during the first 1 – 2 years of observation. Only in the third year could one start to tell the difference and prove that the signal is not produced by a massive BBH of $\mathcal{M}_c \simeq 37 M_{\odot}$ residing in a vacuum environment.

For completeness, we show in Figure 6 the FF derived assuming different values for τ_{gas} . The other model parameters are the same as in Figure 4. As τ_{gas} increases, the FF gets better at later times because the gas effect becomes weaker. We note that when $\tau_{\text{gas}} \gtrsim 5,000$ years, the FF is better than 0.995 for almost five years, which is equivalent to the canonical mission duration of LISA. As a result, LISA may identify our BBHs of a chirp mass of $8.7 M_{\odot}$ as more massive binaries. The measured chirp mass is approximately $18 M_{\odot}$ when $\tau_{\text{gas}} = 5,000$ years and $14 M_{\odot}$ when $\tau_{\text{gas}} = 10^4$ years. In both cases, the overestimation of the mass, and hence the distance (see Eq. (10)), is substantial.

6. DISCUSSIONS

We have seen that those BBHs with $\Gamma = \tau_{\text{gw}}/\tau_{\text{gas}} \gtrsim 1$ could be misidentified by LISA as more massive binaries residing

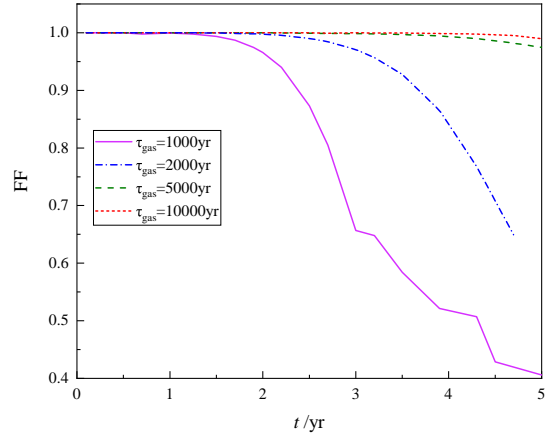


FIG. 6.— Variation of the maximum FF with time assuming different values of τ_{gas} .

in vacuum environments. To what distance could LISA detect such fake massive binaries? The standard way of addressing this question is to derive the maximum distance at which the SNR drops to a threshold, say $\text{SNR} = 10$. This distance is known as the “detection horizon”. In the case without gas, the detection horizon has been derived in several works assuming different LISA configurations. For example, Kyutoku & Seto (2017) showed that

$$d_L \simeq 13 \left(\frac{\mathcal{M}_c}{10 M_{\odot}} \right)^{5/3} \left(\frac{T_{\text{obs}}}{5 \text{ yr}} \right)^{1/2} \left(\frac{\text{SNR}}{10} \right)^{-1} \times \left(\frac{S_n(f)}{10^{-40} \text{ Hz}^{-1}} \right)^{-1/2} \left(\frac{f}{3 \text{ mHz}} \right)^{2/3} \text{ Mpc} \quad (26)$$

for the N2A5 configuration of LISA. Here \mathcal{M}_c and d_L refer to the real chirp mass and real distance of the source.

In fact, the last equation is valid also in the case with gas. This is so because of the following reasons. (i) The stationary phase approximation (Thorne 1987) in which the last equation is derived remains valid, since the evolutionary timescale f/\dot{f} for the frequency is much longer than the GW period $1/f$. We note that \dot{f} here stands for the observed frequency. We dropped the subscript o in \dot{f}_o for simplicity. (ii) In this approximation, the characteristic amplitude defined as $h_c(f) := 2f\tilde{h}(f)$ becomes proportional to $A\dot{f}^{-1/2}$, where A is a function of \mathcal{M}_c , q , f , and d_L , as well as the sky location and orientation of the binary. Noticing that $\dot{f} = \dot{f}_{\text{gw}} + \dot{f}_{\text{gas}} > \dot{f}_{\text{gw}}$, we find that gas in general reduces the characteristic amplitude at any frequency. The reduction is due to a faster drift of the signal in the frequency domain. (iii) Using h_c , we can rewrite the SNR defined in Equation (24) as

$$\text{SNR}^2 = \int_{f_1}^{f_2} \frac{|h_c(f)|^2}{f^2 S_n(f)} df, \quad (27)$$

where f_1 and f_2 denote the minimum and maximum frequencies during the observational period. Because $\Delta f = f_2 - f_1 \ll f$, the integration becomes proportional to $|h_c|^2 \Delta f / (f^2 S_n)$. (iv) In our problem we have $T_{\text{obs}} \ll [f/\dot{f}]$. Therefore, we can write $\Delta f \simeq \dot{f} T_{\text{obs}}$. Again, by noticing that $\dot{f} > \dot{f}_{\text{gw}}$, we find that Δf is broader when gas is present. (v) Finally, the

f^{-1} from the term $|h_c|^2$ cancels the \dot{f} from the term Δf , so that the SNR does not depend on f . Physically, this means the reduction of the characteristic amplitude is compensated by the larger frequency drift.

The above conclusion that gas does not affect the SNR is derived in the scenario of LISA observations. It does not apply to LIGO/Virgo because in the latter case the assumption $T_{\text{obs}} \ll |f/\dot{f}|$ is invalid. In fact, gas will reduce the SNR for LIGO/Virgo sources by suppressing $|h_c|$. Nevertheless, the corresponding change of SNR is small because, as has been explained in §3, the acceleration factor Γ is small when a BBH enters the LIGO/Virgo band.

Therefore, we can use Equation (26) to estimate the detection horizon and, based on it, discuss the detectability of the fake massive BBHs embedded in gaseous environment. For $M_c = 10 M_\odot$, the detection horizon corresponding to a SNR of 10 is approximately 13 Mpc, assuming 5 years of observation. If $M_c = 30 M_\odot$, as the LIGO/Virgo observations tend to suggest (The LIGO Scientific Collaboration & the Virgo Collaboration 2019), the detection horizon elongates to about 80 Mpc.

To estimate the number of fake massive BBHs within the detection horizon, we start from the event rate in the LIGO/Virgo band, which is estimated to be $\mathcal{O}(10^2) \text{ Gpc}^{-3} \text{ yr}^{-1}$ (The LIGO Scientific Collaboration & the Virgo Collaboration 2019). According to this rate, the number of BBHs in the last year before their coalescence is about $N(\tau = 1 \text{ yr}) = 100$ per Gpc^3 , where $\tau = |a/\dot{a}|$ denotes the orbital evolutionary timescale. For the other BBHs at an earlier evolutionary stage,

we can follow the continuity equation (e.g., see Sec. V in Amaro-Seoane 2019) and derive that $dN/d \ln a \propto \tau$. In our problem, $\tau = (1/\tau_{\text{gw}} + \tau_{\text{gas}})^{-1}$. At a frequency of $f = 3$ mHz, where LISA is the most sensitive, $\tau_{\text{gw}} \simeq (1500 - 9000)$ years when M_c varies from $30 M_\odot$ to $10 M_\odot$. (i) Without gas, $\tau = \tau_{\text{gw}}$, and we find that the number density of BBHs at $f \sim 3$ mHz is about $(1.5 - 9) \times 10^5 \text{ Gpc}^{-3}$. The number of BBHs inside the detection horizon is 8–320. (ii) With gas, the number would be smaller because τ is shortened by gas friction. In the extreme case that all BBHs are embedded in gas, if we assume $\tau_{\text{gas}} = 10^3$ years, we find that $\tau \simeq (600 - 900)$ years when M_c varies from $30 M_\odot$ to $10 M_\odot$. Correspondingly, the number density of BBHs at $f \sim 3$ mHz is $(6 - 9) \times 10^4 \text{ Gpc}^{-3}$. The number of BBHs inside the detection horizon decreases to 0.8–130, but is not zero.

Since BBHs embedded in gaseous environments could be common, the effect of hydrodynamics should be considered more carefully in the waveform modeling. Otherwise, as our results suggest, LISA may provide a biased demography of BBHs. Such a bias may also affect future cosmology studies, given the possibility of using BBHs as standard sirens to measure cosmological parameters.

Acknowledgement.—This work is supported by the NSFC grants No. 11873022 and 11991053. XC is supported partly by the Strategic Priority Research Program “Multi-wavelength gravitational wave universe” of the Chinese Academy of Sciences (No. XDB23040100 and XDB23010200). The computation in this work was performed on the High Performance Computing Platform of the Center for Life Science, Peking University.

REFERENCES

- Abbott, B. P., Abbott, R., Abbott, T. D., Abernathy, M. R., Acernese, F., Ackley, K., Adams, C., Adams, T., Addesso, P., Adhikari, R. X., & et al. 2016, *ApJ*, 818, L22
- Amaro-Seoane, P. 2019, *Phys. Rev. D*, 99, 123025
- Amaro-Seoane, P., Audley, H., Babak, S., Baker, J., Barausse, E., Bender, P., Berti, E., Binetruy, P., Born, M., Bortoluzzi, D. et al. 2017, *arXiv:1702.00786*
- Antoni, A., MacLeod, M., & Ramirez-Ruiz, E. 2019, *ApJ*, 884, 22
- Barausse, E., Cardoso, V., & Pani, P. 2014, *Phys. Rev. D*, 89, 104059
- Bartos, I., Kocsis, B., Haiman, Z., & Márka, S. 2017, *ApJ*, 835, 165
- Bondi, H. 1952, *MNRAS*, 112, 195
- Broadhurst, T., Diego, J. M., & Smoot, George, I. 2018, *arXiv e-prints*, *arXiv:1802.05273*
- Cardoso, V. & Maselli, A. 2019, *arXiv e-prints*, *arXiv:1909.05870*
- Chamberlain, K., Moore, C. J., Gerosa, D., & Yunes, N. 2019, *Phys. Rev. D*, 99, 024025
- Chen, X. & Amaro-Seoane, P. 2017, *ApJ*, 842, L2
- Chen, X. & Han, W.-B. 2018, *Communications Physics*, 1, 53
- Chen, X., Li, S., & Cao, Z. 2019, *MNRAS*, 485, L141
- Chen, X. & Shen, Z. 2019, *Proceedings*, 17, 4
- Cutler, C. & Flanagan, É. E. 1994, *Phys. Rev. D*, 49, 2658
- D’Orazio, D. J. & Loeb, A. 2018, *Phys. Rev. D*, 97, 083008
- Escala, A., Larson, R. B., Coppi, P. S., & Mardones, D. 2004, *ApJ*, 607, 765
- Fang, Y., Chen, X., & Huang, Q.-G. 2019, *ApJ*, 887, 210
- Fedrow, J. M., Ott, C. D., Spherhake, U., Blackman, J., Haas, R., Reisswig, C., & De Felice, A. 2017, *Phys. Rev. Lett.*, 119, 171103
- Finn, L. S. 1992, *Phys. Rev. D*, 46, 5236
- Ginat, Y. B., Glanz, H., Perets, H. B., Grishin, E., & Desjacques, V. 2020, *MNRAS*
- Haiman, Z., Kocsis, B., & Menou, K. 2009, *ApJ*, 700, 1952
- Hannuksela, O. A., Haris, K., Ng, K. K. Y., Kumar, S., Mehta, A. K., Keitel, D., Li, T. G. F., & Ajith, P. 2019, *The Astrophysical Journal*, 874, L2
- Hoang, B.-M., Naoz, S., Kocsis, B., Farr, W. M., & McIver, J. 2019, *ApJ*, 875, L31
- Inayoshi, K., Tamanini, N., Caprini, C., & Haiman, Z. 2017, *Phys. Rev. D*, 96, 063014
- Ivanova, N., Justham, S., Chen, X., De Marco, O., Fryer, C. L., Gaburov, E., Ge, H., Glebbeek, E., Han, Z., Li, X.-D., Lu, G., Marsh, T., Podsiadlowski, P., Potter, A., Soker, N., Taam, R., Tauris, T. M., van den Heuvel, E. P. J., & Webbink, R. F. 2013, *A&A Rev.*, 21, 59
- Kim, H. & Kim, W.-T. 2007, *ApJ*, 665, 432
- Kim, H., Kim, W.-T., & Sánchez-Salcedo, F. J. 2008, *ApJ*, 679, L33
- Klein, A., Barausse, E., Sesana, A., Petiteau, A., Berti, E., Babak, S., Gair, J., Aoudia, S., Hinder, I., Ohme, F., & Wardell, B. 2016, *Phys. Rev. D*, 93, 024003
- Kocsis, B., Yunes, N., & Loeb, A. 2011, *Phys. Rev. D*, 84, 024032
- Kremer, K., Chatterjee, S., Breivik, K., Rodriguez, C. L., Larson, S. L., & Rasio, F. A. 2018, *Phys. Rev. Lett.*, 120, 191103
- Kyutoku, K. & Seto, N. 2016, *MNRAS*, 462, 2177
- . 2017, *Phys. Rev. D*, 95, 083525
- Lamberts, A., Garrison-Kimmel, S., Hopkins, P. F., Quataert, E., Bullock, J. S., Faucher-Giguère, C. A., Wetzel, A., Kereš, D., Drango, K., & Sanderson, R. E. 2018, *MNRAS*, 480, 2704
- Lindblom, L., Owen, B. J., & Brown, D. A. 2008, *Phys. Rev. D*, 78, 124020
- Loeb, A. 2016, *ApJ*, 819, L21
- MacLeod, M., Antoni, A., Murguía-Berthier, A., Macias, P., & Ramirez-Ruiz, E. 2017, *The Astrophysical Journal*, 838, 56
- McKernan, B., Ford, K. E. S., Lyra, W., & Perets, H. B. 2012, *MNRAS*, 425, 460
- Meiron, Y., Kocsis, B., & Loeb, A. 2017, *ApJ*, 834, 200
- Miller, M. C. 2002, *ApJ*, 581, 438
- Moore, C. J., Gerosa, D., & Klein, A. 2019, *MNRAS*, 488, L94
- Nakamura, T. T. 1998, *Phys. Rev. Lett.*, 80, 1138
- Ostriker, E. C. 1999, *ApJ*, 513, 252
- Peters, P. C. 1964, *Physical Review*, 136, 1224
- Randall, L. & Xianyu, Z.-Z. 2019, *arXiv:1902.08604*
- Robson, T., Cornish, N. J., Tamanini, N., & Toonen, S. 2018, *Phys. Rev. D*, 98, 064012
- Sánchez-Salcedo, F. J. & Brandenburg, A. 1999, *ApJ*, 522, L35
- . 2001, *MNRAS*, 322, 67
- Sathyaprakash, B. S. & Schutz, B. F. 2009, *Living Reviews in Relativity*, 12, 2
- Schutz, B. F. 1986, *Nature*, 323, 310

- Sereno, M., Jetzer, P., Sesana, A., & Volonteri, M. 2011, *MNRAS*, 415, 2773
- Sesana, A. 2016, *Physical Review Letters*, 116, 231102
- Seto, N. 2002, *MNRAS*, 333, 469
- . 2004, *Phys. Rev. D*, 69, 022002
- Smith, G. P., Jauzac, M., Veitch, J., Farr, W. M., Massey, R., & Richard, J. 2018, *MNRAS*, 475, 3823
- Stone, N. C., Metzger, B. D., & Haiman, Z. 2017, *MNRAS*, 464, 946
- Tagawa, H., Saitoh, T. R., & Kocsis, B. 2018, *Phys. Rev. Lett.*, 120, 261101
- Takahashi, R. & Nakamura, T. 2003, *ApJ*, 595, 1039
- Tamanini, N., Klein, A., Bonvin, C., Barausse, E., & Caprini, C. 2020, *Phys. Rev. D*, 101, 063002
- The LIGO Scientific Collaboration & the Virgo Collaboration. 2019, *Physical Review X*, 9, 031040
- Thorne, K. S. *Gravitational radiation.*, ed. , S. W. Hawking W. Israel (Cambridge University Press), 330–458
- Torres-Orjuela, A., Chen, X., & Amaro-Seoane, P. 2020, arXiv e-prints, arXiv:2001.00721
- Wong, K. W. K., Baibhav, V., & Berti, E. 2019, *MNRAS*, 488, 5665
- Yunes, N., Kocsis, B., Loeb, A., & Haiman, Z. 2011, *Phys. Rev. Lett.*, 107, 171103